

## Article

# Preparation and Properties of Attapulгите-Hydroxyethyl Cellulose Composite Poly (Acrylic Acid-co-2-acrylamide-2-methylpropanesulfonic Acid) Concrete Internal Curing Material

Yunan Zhao <sup>1</sup>, Laifa Wang <sup>2</sup>, Yongqing Li <sup>2</sup>, Rui Xiong <sup>3</sup> and Fuyang Lu <sup>3,\*</sup>

<sup>1</sup> Qinghai Guoluo Highway Engineering Construction Co., Ltd., Xining 810008, China; younanzhao6@outlook.com

<sup>2</sup> Qinghai Traffic Control Construction Engineering Group Co., Ltd., Xining 810003, China

<sup>3</sup> School of Materials Science and Engineering, Chang'an University, Xi'an 710061, China; xiongrui@chd.edu.cn

\* Correspondence: lufuyang@chd.edu.cn

**Abstract:** Attapulгите-hydroxyethyl cellulose-poly (acrylic acid-co-2-acrylamide-2-methylpropanesulfonic acid) (ATP-HEC-P(AA-co-AMPS)) in-concrete curing material was synthesized by aqueous solution polymerization using attapulгите (ATP) as an inorganic filler and hydroxyethyl cellulose (HEC) as a backbone. The effects of relevant factors such as ATP dosage, HEC dosage, degree of neutralization, initiator quality, and cross-linking agent quality on the water absorption characteristics of ATP-HEC-P (AA-co-AMPS) were investigated through expansion tests. The micro-morphology of ATP-HEC-P (AA-co-AMPS) was also comprehensively characterized using Fourier transform infrared spectroscopy, scanning electron microscopy, a thermal analysis, and other applicable means. The results showed that the prepared ATP-HEC-P (AA-co-AMPS) had a strong water absorption and water retention capacity, with a water absorption multiplicity of 382 g/g in deionized water and 21.55% water retention capacity after being placed at room temperature for 7 d in a bare environment. Additionally, ATP-HEC-P (AA-co-AMPS) showed good performance for absorbing liquids within the pH range of 7–12. The material's thermal stability and mechanical properties were also significantly improved after the addition of ATP. The preparation cost is low, the process is simple, and the material meets the requirements for concrete curing materials.

**Keywords:** concrete; internal curing; polymer; attapulгите; carboxyethyl cellulose



**Citation:** Zhao, Y.; Wang, L.; Li, Y.; Xiong, R.; Lu, F. Preparation and Properties of Attapulгите-Hydroxyethyl Cellulose Composite Poly (Acrylic Acid-co-2-acrylamide-2-methylpropanesulfonic Acid) Concrete Internal Curing Material. *Buildings* **2024**, *14*, 1467. <https://doi.org/10.3390/buildings14051467>

Academic Editor: Binsheng (Ben) Zhang

Received: 2 April 2024  
Revised: 14 May 2024  
Accepted: 15 May 2024  
Published: 18 May 2024



**Copyright:** © 2024 by the authors. Licensee MDPI, Basel, Switzerland. This article is an open access article distributed under the terms and conditions of the Creative Commons Attribution (CC BY) license (<https://creativecommons.org/licenses/by/4.0/>).

## 1. Introduction

A concrete internal curing material is a cross-linked polymer containing numerous hydrophilic groups within a three-dimensional network structure [1,2], enabling rapid absorption of a substantial water volume to form a gel. The water-absorbing capacity can reach hundreds or even thousands of times its weight [3–5], demonstrating excellent water retention performance even under specific pressure conditions. These concrete internal curing materials find widespread application in agriculture [6], health care [7], environmental protection [8], construction [9], daily use chemicals [10], and various other fields [11]. Current research has shown that the introduction of high water-absorbing resins into concrete can improve the frost resistance, impermeability, and cracking resistance of concrete.

According to the source of materials, concrete internal curing materials are primarily categorized into two groups: synthetic polymer systems and natural polymer-modified systems [12,13]. Nevertheless, traditional highly absorbent materials exhibit drawbacks such as high cost, non-degradability, and limited water absorption in the presence of high-concentration electrolytes [14,15]. The current market application of concrete internal curing materials is mainly acrylic polymer. Simple acrylic acid copolymerization into a high water absorption polymer results in good water absorption but poor salt resistance, limiting the scope of practical applications. However, it can be copolymerized with

non-ionic groups (such as acrylamide) to improve the salt-resistant properties of water-absorbing polymers [16,17]. To address the shortcomings of traditional synthetic high water-absorbent polymers, natural polysaccharide-modified water-absorbent materials, including cellulose [18,19], starch [20], sodium alginate [21], and chitosan [11], have been developed in recent years. These water-absorbent materials possess advantages such as degradability, renewability, good affinity, low cost, etc., resulting in better application prospects. At present, concrete internal maintenance usually involves acrylic and other organic polymer materials. Inorganic components are introduced into the polymer to improve the absorbing liquid ability in ionic solutions, and can improve the mechanical properties of the material, but at present, the development of organic/inorganic composite internal maintenance materials is relatively slow.

HEC is a material containing polyhydroxy groups with particular water-absorbing abilities, and it has a large specific surface area and many internal capillaries [22]. It is also non-toxic, low-cost, renewable, widely available, biocompatible, and biodegradable [23]. Therefore, a composite water-absorbent material prepared from it exhibits good water absorption and is significant for environmental protection. AMPS is a solid anionic water-soluble monomer containing strong hydrophilic groups with good salt resistance, acid-base resistance, and hydrolytic stability [17,24]. ATP is an aqueous magnesium–aluminum-rich layered chain silicate mineral with a particular fibrous crystal structure and a large surface area, having a theoretical chemical formula of  $Mg_5Si_8O_{20}(HO)_2(OH)_4 \cdot 4H_2O$  [25,26]. The surface of ATP contains a large amount of reactive Si-OH, which can be further activated through heating and acid treatment [27]. This process changes the physico-chemical properties of ATP, enabling its composition with organic materials to prepare organic–inorganic composites. Many studies have shown that the liquid-absorbent properties, mechanical properties, and thermal stability of water-absorbent polymers are significantly improved after the addition of ATP.

In this experiment, concrete internal curing materials (ATP-HEC-P (AA-co-AMPS)) were prepared through aqueous solution polymerization using HEC as the backbone to form an interpenetrating network structure. AA and AMPS were employed as hydrophilic modified monomers to introduce hydrophilic groups, and the polymers were doped with ATP to form an inorganic composite. The optimal synthesis scheme was determined by studying different experimental variables, and the polymers were structurally characterized and tested using FTIR, SEM, and thermal analyses.

## 2. Materials and Methods

### 2.1. Materials

The used materials were as follows: acrylic acid (AA) from Tianjin Damao Chemical Reagent Factory, Tianjin, China; ethanol from Tianjin Damao Chemical Reagent Factory, Tianjin, China; 2-acrylamido-2-methylpropane sulfonic acid (AMPS) from Shanghai McLean Biochemical Technology Co., Ltd., Shanghai, China; methylene-bis-acrylamide (MBA) from Shanghai McLean Biochemical Technology Co., Ltd., Shanghai, China; ammonium persulfate (APS) from Shanghai McLean Biochemical Technology Co., Ltd., Shanghai, China; hydroxyethyl Cellulose (HEC) from Shanghai McLean Biochemical Technology Co., Ltd., Shanghai, China; NaCl from Shanghai McLean Biochemical Technology Co., Ltd., Shanghai, China;  $Ca(OH)_2$  from Shanghai McLean Biochemical Technology Co., Ltd., Shanghai, China; sodium dodecyl sulfate (SDS) from Shanghai McLean Biochemical Technology Co., Ltd., Shanghai, China; and attapulgite (ATP) from Jiangsu Province. All the experimental chemicals were analytically pure except for attapulgite, and all experimental water was deionized water.

### 2.2. Preparation of ATP-HEC-P (AA-co-AMPS) Concrete Internal Curing Material

The appropriate amount of HEC, ATP, SDS, and water were put into a beaker and stirred at 70 °C for 45 min to produce a dispersed emulsion. The dispersed emulsion was cooled down to 40 °C and an APS solution (5 mL) was added dropwise, stirring for 10 min.



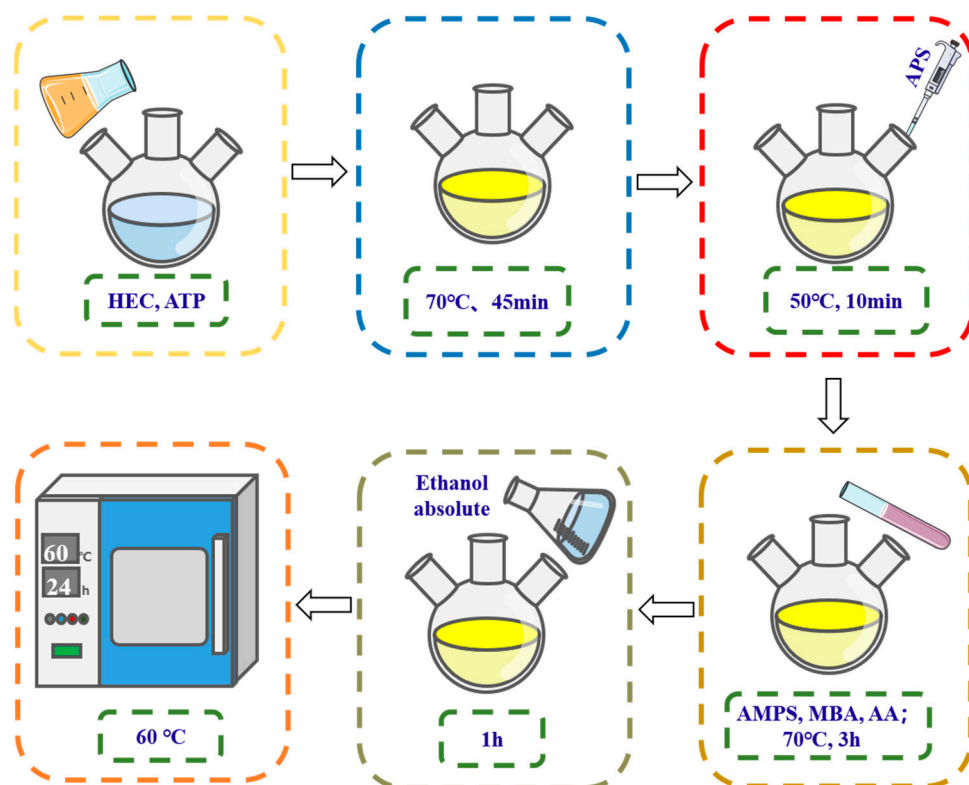


**Figure 2.** Flowchart of ATP-HEC-P (AA-co-AMPS) preparation.

### 2.3. Methods

#### 2.3.1. SEM and EDS

To observe the microscopic morphology of the synthesized polymers, the powders were subjected to a Hitachi E-1045 gold spraying treatment and observed using a Hitachi S-4800 scanning electron microscope (Tokyo, Japan). The elemental distribution in the sample was measured by an EDS energy spectrometer.

#### 2.3.2. FT-IR

The transmission infrared spectra of the samples were recorded in a wavelength range of 4000 to 400  $\text{cm}^{-1}$  using a Bruker TENSOR II FTIR spectrometer (Billerica, MA, USA).

#### 2.3.3. Thermodynamic Analysis

The thermodynamic analysis of the synthesized polymers was carried out using the TA SDT 650 simultaneous thermal analyzer test. The test temperature range was 30–600  $^{\circ}\text{C}$ , and the heating rate was 10  $^{\circ}\text{C}/\text{min}$ . The test environment was nitrogen-protected.

#### 2.3.4. Measurement of Swelling Behavior

In the experiment, 0.1 g of synthesized polymer was placed into a unique filter bag and then immersed in a beaker with 500 mL of deionized water, tap water, 0.9% NaCl solution, and a saturated  $\text{Ca}(\text{OH})_2$  solution, respectively. The system was left to stand at room temperature. The masses of the absorbed polymer were measured at different time intervals, and the multiplicities of water absorption of the different solutions were calculated using a specific equation:

$$Q = (M_2 - M_1)/M_1 \quad (1)$$

where  $M_1$  and  $M_2$  are the masses of the dry and absorbed polymer, respectively, and  $Q$  (g/g) is the water absorption multiplicity [28].

### 2.3.5. Determination of Water Retention at Different Temperatures

In the experiment, 0.1 g of synthesized polymer was weighed and put into deionized water to reach dissolution equilibrium. Then, they were reweighed and placed in an environmental chamber at 20 °C, 30 °C, 40 °C, and 50 °C several times. The weighing was performed at intervals, and the water retention multiplicity was calculated at different temperatures using the following equation:

$$R = (M_3 - M_1)/(M_2 - M_1) \quad (2)$$

where  $M_1$  is the mass of the dry polymer,  $M_2$  is the mass of the polymer after reaching dissolution equilibrium, and  $M_3$  is the mass of the polymer after water loss.

### 2.3.6. Repeated Swelling Performance Test

The polymer was saturated using deionized water and the mass of water absorbed was recorded. Then, it was dried in an oven (60 °C) to a constant weight. This water absorption–drying step was repeated for calculating the water absorption multiple each time.

### 2.3.7. pH Dynamic Perception Test

An amount of 0.1 g of the polymer sample was weighed and immersed in 0.9% NaCl solution. The pH of the solution was adjusted with NaOH. The swelling multiplicity was then measured at pH 7–12.

### 2.3.8. Stress–Strain Curve Testing

The unpolymerized in-concrete curing agent was poured into a 10 mm diameter cylindrical mold, removed at the end of the reaction, and the compression characteristics of the in-concrete curing agent were analyzed using a mass spectrometer, with a compression rate of 2 mm/s, a trigger pressure of 0.05 Newton, and a compression set of 50%.

## 3. Results

### 3.1. Effect of Synthesis Conditions on Liquid Absorption Capacity

#### 3.1.1. The Effect of AMPS Content on the Ability of ATP-HEC-P (AA-co-AMPS) to Absorb Liquids

The synthesizing factor variables were explored using 5 mL of AA monomer as the substrate to facilitate the study. The effect of AMPS content on the wicking ability of ATP-HEC-P (AA-co-AMPS) is shown in Figure 3a. From the figure, it can be seen that the liquid-absorbing capacity of ATP-HEC-P (AA-co-AMPS) in deionized water, tap water, 0.9% NaCl solution, and a saturated  $\text{Ca}(\text{OH})_2$  solution has a similar pattern of change. The liquid-absorbing ability of ATP-HEC-P (AA-co-AMPS) in different solutions is enhanced when the AMPS content increases from 1.3767 g to 1.5767 g. This is because the number of hydrogen bonds formed between hydrophilic groups and water molecules in ATP-HEC-P (AA-co-AMPS) increases with an increase in the AMPS content, which improves the liquid-absorbing ability of ATP-HEC-P (AA-co-AMPS) [29]. However, when the content of AMPS continues to increase, the hydrophilic groups become too numerous, and significant hydrogen bonding between molecules leads to a contraction of the three-dimensional network structure. This, in turn, decreases the liquid-absorbing capacity of ATP-HEC-P (AA-co-AMPS).

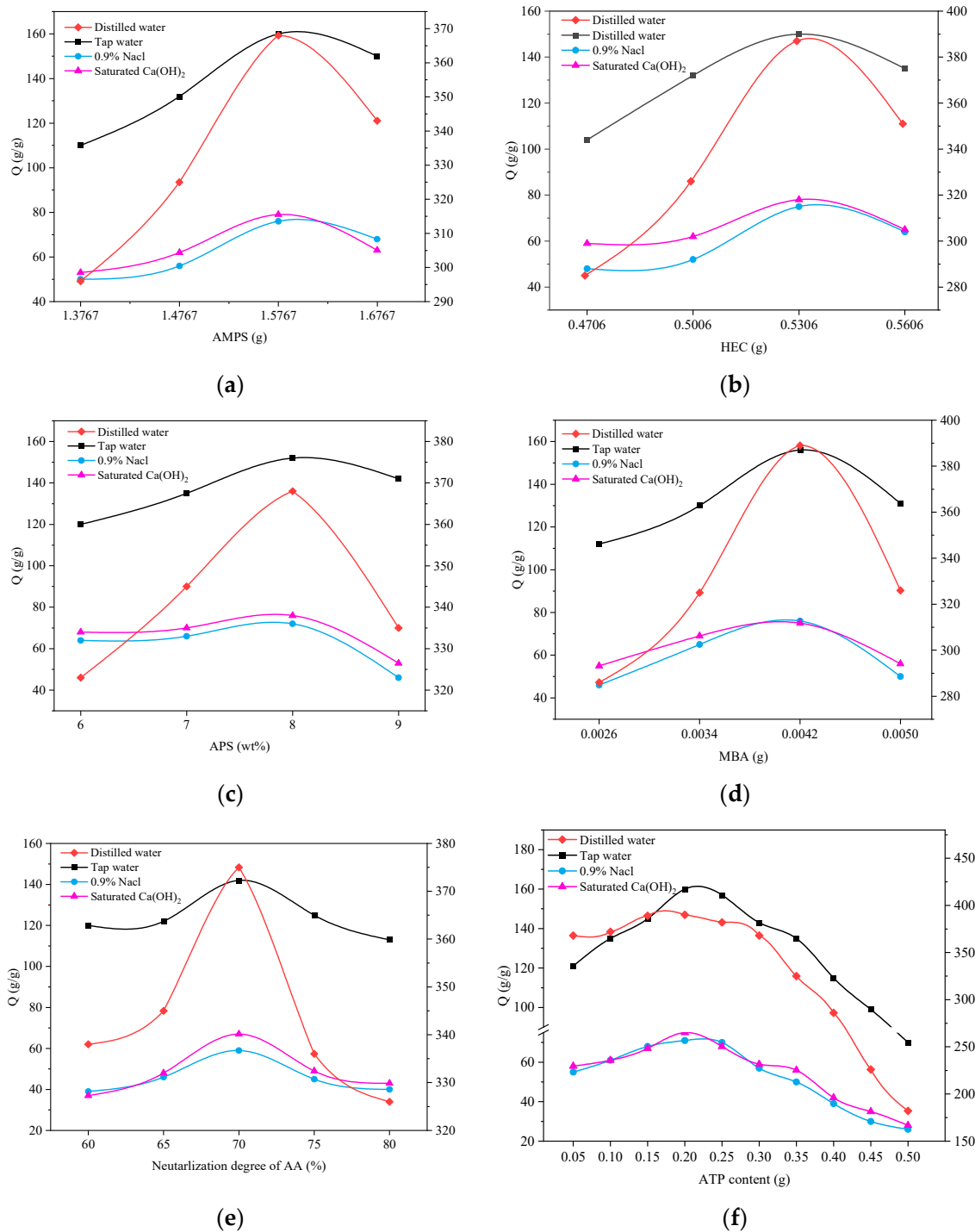


**Figure 3.** Effects of synthetic factors on ATP-HEC-P(AA-co-AMPS) concrete internal curing materials: (a) AMPS content, (b) HEC content, (c) APS content, (d) MBA content, (e) neutralization degree of AA, and (f) ATP content.

### 3.1.2. The Effect of HEC Content on the Ability of ATP-HEC-P (AA-co-AMPS) to Absorb Liquids

Figure 3b shows the effect of HEC content on the liquid absorption capacity of ATP-HEC-P (AA-co-AMPS). As can be seen from the figure, the liquid absorption capacity of ATP-HEC-P (AA-co-AMPS) tended to increase first and then decreased with the increase in HEC content. In the synthesis reaction, HEC plays the role of the skeleton, and the active sites in HEC react with the active radicals on the polymer chain of P (AA-co-AMPS)

to entangle with each other and form an interpenetrating network structure [30]. When the content of HEC is low, the number of active sites in the system is small, which is unfavorable to the formation of the interpenetrating network structure, and the stability of ATP-HEC-P (AA-co-AMPS) is poor after liquid absorption. However, when the HEC content is high, the interpenetrating network structure is more compact, and the liquid absorption capacity becomes poor due to the increased number of active sites in the system.

### 3.1.3. The Effect of APS Content on the Ability of ATP-HEC-P (AA-co-AMPS) to Absorb Liquids

Figure 3c shows the effect of APS content on the wicking capacity of ATP-HEC-P (AA-co-AMPS). During the reaction, APS acts as an initiator and affects the length of the P (AA) and P (AMPS) molecular chains. As can be seen from the figure, when the APS solution is lower than 8 wt%, the initiating effect on the reaction is lower due to the low content of APS, and the polymerized molecular chains are shorter and have a weaker ability to absorb liquid. However, when the APS solution is greater than 8 wt%, the active radical sites in the system increase, the reaction is intense, the cross-linking density increases, the interpenetrating network structure is more compact, and the liquid-absorbing ability worsens.

### 3.1.4. The Effect of MBA Content on the Ability of ATP-HEC-P (AA-co-AMPS) to Absorb Liquids

MBA serves as a cross-linker in the reaction, facilitating the cross-linking of HEC and P (AA-co-AMPS) polymer chains. Figure 3d illustrates the impact of MBA content on the liquid-absorbing capability of ATP-HEC-P (AA-co-AMPS). The optimal MBA content in the reaction is determined to be 0.0042 g. If MBA content falls below 0.0042 g, the liquid absorption ability will suffer due to a reduced number of cross-linking sites and a lower cross-linking density within the system. This hinders the formation of an interpenetrating network structure [31]. Exceeding 0.0042 g, MBA results in an overly large cross-linking density within the system, impeding the extension of polymer chains and the formation of a network structure. Consequently, the liquid absorption ability diminishes.

### 3.1.5. The Effect of AA Neutralization on the Suction Capacity of ATP-HEC-P (AA-co-AMPS)

Figure 3e illustrates the impact of the AA neutralization degree on the liquid-absorbing capacity of ATP-HEC-P (AA-co-AMPS). NaOH neutralization of AA results in the formation of  $C_3H_3O_2Na$ , and  $-COOH$  in AA transforms into  $-COONa$ , enhancing the swelling capacity of ATP-HEC-P (AA-co-AMPS) due to the electrostatic force within the network. Increasing the neutralization degree of AA from 60% to 70% results in a significant improvement in liquid absorption ability, particularly in 0.9% NaCl and saturated  $Ca(OH)_2$  solutions. Additionally, the material exhibits significantly enhanced salt resistance. A continuous increase in the neutralization degree leads to an excess of  $Na^+$  in the system, exerting a shielding effect. This effect diminishes electrostatic repulsion, resulting in a decrease in liquid-absorbing ability.

### 3.1.6. The Effect of ATP Content on the Ability of ATP-HEC-P (AA-co-AMPS) to Absorb Liquids

Figure 3f depicts the impact of ATP content on the liquid-absorbing capacity of ATP-HEC-P (AA-co-AMPS). Increasing ATP content from 0.05 g to 0.20 g results in an upward trend in liquid-absorbing capacity for ATP-HEC-P (AA-co-AMPS). However, surpassing 0.20 g of ATP content leads to a decline in liquid-absorbing capacity, particularly evident when the content exceeds 0.30 g. ATP does not enhance the liquid-absorbing capacity of ATP-HEC-P (AA-co-AMPS); rather, it has a detrimental effect. This occurs because the  $-OH$  on the surface of ATP participates in the reaction process, contributing to the formation of a more effective water-absorbing network structure. However, with higher ATP content, the free ATP outside the network structure increases, leading to the clogging of the network structure and a subsequent reduction in liquid-absorbing capacity.

The subsequent experiments were conducted using the optimal experimental parameters, which included 1.5765 g of AMPS, 0.5306 g of HEC, 8 wt% of APS, 0.0042 g of MBA, 70% AA neutralization, and 0.20 g of ATP.

### 3.2. Physical Characterization

The samples were dried and pulverized before and after ATP modification for direct observation. As depicted in Figure 4, it is evident that the color of HEC-P (AA-co-AMPS) was whitish prior to the addition of ATP. Conversely, after the incorporation of ATP, the color of ATP-HEC-P (AA-co-AMPS) turned light yellow, resembling the color of ATP itself. Furthermore, in the investigation of ATP content variation in Section 3.1.6, it was observed that the color of the samples deepened with increasing ATP content. These findings indicate the successful grafting of ATP onto HEC-P (AA-co-AMPS) by following the samples' ethanol soaking and deionized water rinsing, resulting in a noticeable color change in the samples.



**Figure 4.** Sample photos: (a) HEC-(AA-co-AMPS) and (b) ATP-HEC-P (AA-co-AMPS).

### 3.3. SEM and EDS

SEM images of HEC-P (AA-co-AMPS) and ATP-HEC-P (AA-co-AMPS) are presented in Figure 5, respectively. HEC-P (AA-co-AMPS) exhibits irregularly distributed laminar flakes on its surface, which are relatively smooth and loose. In contrast, ATP-HEC-P (AA-co-AMPS), after the addition of ATP, exhibits a distribution of crushed small particles with a rough surface and large pores. This morphology is conducive to the diffusion of water molecules into the material's interior, thereby enhancing its liquid absorption capacity. Additionally, this observation provides evidence of ATP's involvement in the polymerization reaction process.

An EDS spectrometer measured the elemental contents of HEC-P (AA-co-AMPS) and ATP-HEC-P (AA-co-AMPS) at the same magnification. The EDS energy spectra are shown in Figure 6, and the elemental content results are shown in Table 1. It can be found that the elemental contents of Mg and Si in the polymers increased significantly before and after the addition of ATP, which indicates that ATP has been successfully introduced into HEC-P (AA-co-AMPS).

**Table 1.** EDS elemental content test results.

| Element                | C (At%) | O (At%) | Al (At%) | Mg (At%) | Si (At%) |
|------------------------|---------|---------|----------|----------|----------|
| HEC-P (AA-co-AMPS)     | 68.8    | 31.1    | 0.1      | -        | -        |
| ATP-HEC-P (AA-co-AMPS) | 59.2    | 40.1    | 0.1      | 0.3      | 0.3      |

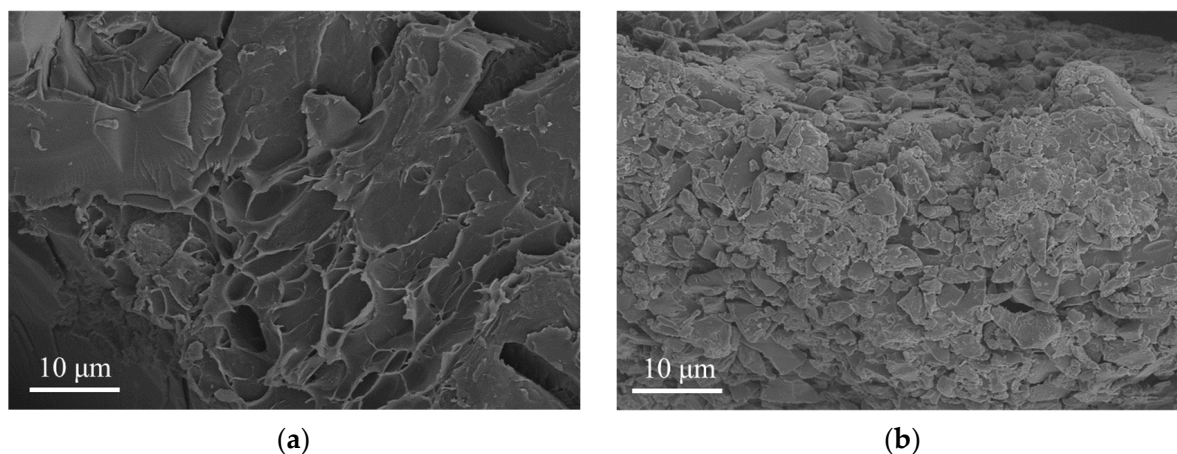


**Figure 5.** Scanning electron microscopies: (a) HEC-(AA-co-AMPS) and (b) ATP-HEC-P (AA-co-AMPS).

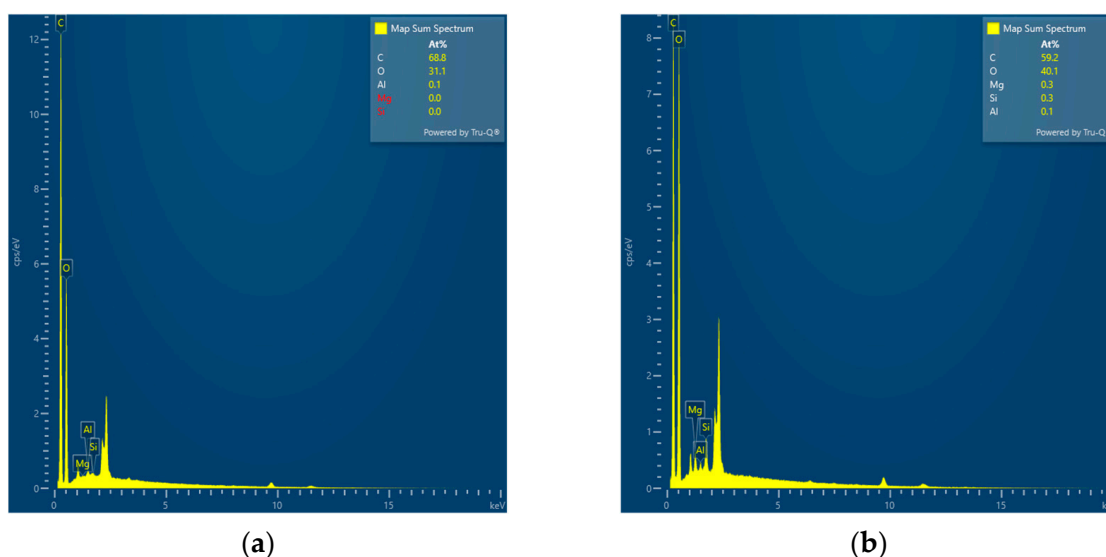


**Figure 6.** EDS spectra: (a) P (HEC-AA-AMPS) and (b) ATP-BF-P (HEC-AA-AMPS).

### 3.4. FT-IR

Figure 7 shows the FT-IR profiles of HEC and ATP-HEC-P (AA-co-AMPS). In the infrared spectra of ATP-HEC-P (AA-co-AMPS), the C-O-C stretching vibration peak on HEC at  $915\text{ cm}^{-1}$  [32] and the planar peak of C-OH at  $1336\text{ cm}^{-1}$  disappear, after the polymerization reaction. The absorption peak at  $2925\text{ cm}^{-1}$ , attributed to the aliphatic stretching vibration of C-H on HEC, still exists in ATP-HEC-P (AA-co-AMPS) [33]. Meanwhile, the peak at  $3433\text{ cm}^{-1}$ , attributed to the O-H stretching vibration on HEC, is slightly lower in intensity compared to the absorption peak of ATP-HEC-P (AA-co-AMPS) [34]. These results suggest that HEC is involved in the chemical reaction. In the FTIR curves of ATP-HEC-P (AA-co-AMPS), the telescopic vibration absorption peak of O=S at  $628\text{ cm}^{-1}$ , the asymmetric telescopic vibration peak of -COO- at  $1404\text{ cm}^{-1}$ , and the telescopic vibration peak of C=O in the amide group at  $1642\text{ cm}^{-1}$  are observed [35]. These observations indicate that the poly (acrylic acid) chain and AMPS are successfully grafted onto the HEC backbone. Additionally, Si-O-Si bending vibrational peaks of inorganic minerals at  $800\text{ cm}^{-1}$  are identified [36], suggesting the involvement of inorganic minerals in graft co-polymerization.

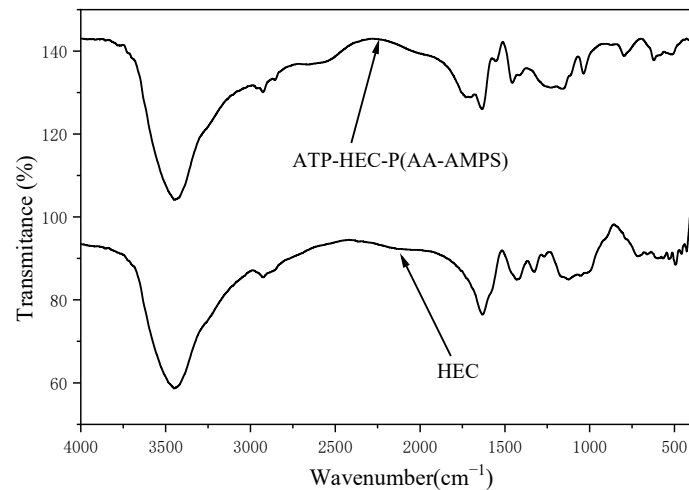


**Figure 7.** FT-IR test pattern.

### 3.5. Thermal Stability Analysis

TG/DTG curves for ATP, HEC-P (AA-co-AMPS), and ATP-HEC-P (AA-co-AMPS) are presented in Figure 8. The TG decomposition curves of ATP display three steps, occurring at 30 °C to 119 °C, 119 °C to 242 °C, and 242 °C to 600 °C. The weight losses are 6.20%, 2.93%, and 5.63%, respectively. Simultaneously, three peaks on the DTG curve at 97 °C, 216 °C, and 273 °C correspond to the first three stages, indicating the maximum decomposition rate.

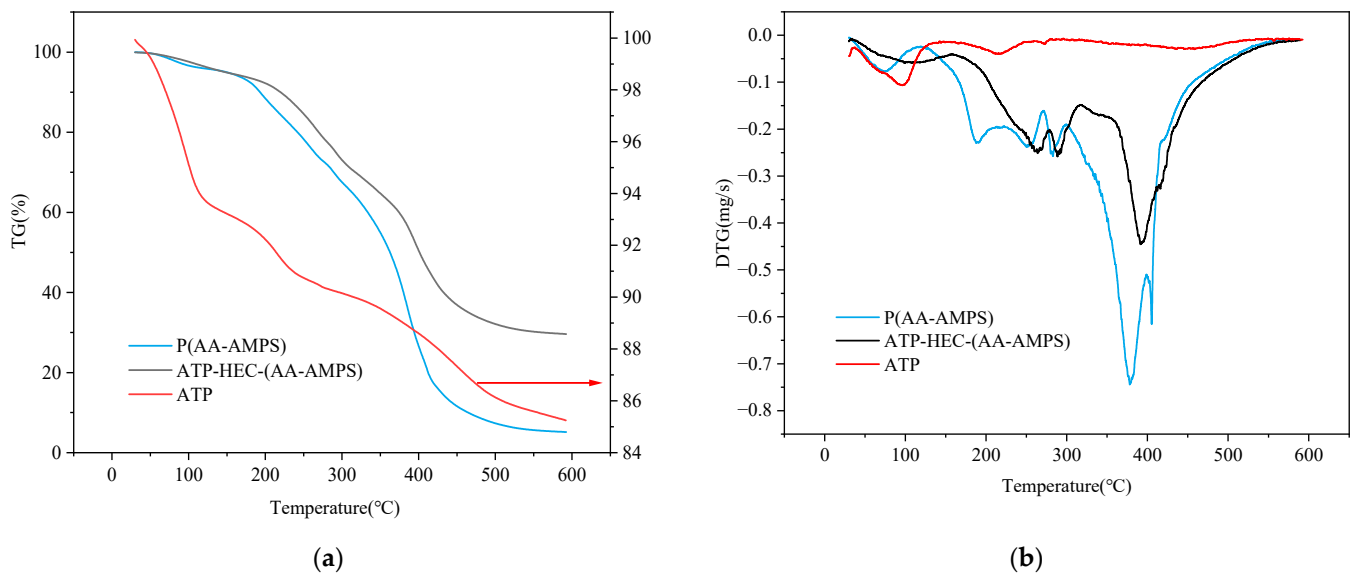


**Figure 8.** TG-DTG curves of samples: (a) TG curves and (b) DTG curves.

The thermal decompositions of HEC-P (AA-co-AMPS) and ATP-HEC-P (AA-co-AMPS) are similarly divided into three steps. The corresponding temperature intervals of 30 °C to 170 °C, 170 °C to 417 °C, 417 °C to 600 °C, and 30 °C to 204 °C, 204 °C to 439 °C, 439 °C to 600 °C, result in mass loss ratios of 5.96%, 76.13%, 12.76%, and 8.12%, 54.18%, 8.08%. The initial stage primarily involves the decomposition of water and unreacted raw materials in the composite absorbent material. The majority of mass loss occurs in the second stage due to the decomposition of oligomers in the material and branched chains in the polymer. The mass loss in the third stage is attributed to the decomposition of the leading chains in the polymers and the disruption of the three-dimensional network structure. Additionally, it is noteworthy that ATP-HEC-P (AA-co-AMPS) exhibits lower mass loss than HEC-P

(AA-co-AMPS) across the entire temperature range, indicating that the incorporation of ATP enhances the material's thermal stability.

### 3.6. Measurement of Swelling Behavior

Figure 9a illustrates the swelling test of ATP-HEC-P (AA-co-AMPS) in various solutions. The water absorption capacities of ATP-HEC-P (AA-co-AMPS) in deionized water, tap water, 0.9% NaCl solution, and a saturated  $\text{Ca}(\text{OH})_2$  solution are recorded as 382 g/g, 142 g/g, 57 g/g, and 73 g/g, respectively, after 120 min. Notably, ATP-HEC-P (AA-co-AMPS) reaches 87.69%, 88.73%, 73.68%, and 72.60% of their maximum swelling rates within 15 min, respectively, and generally attains equilibrium swelling between 30 and 60 min. This indicates that the liquid is absorbed quickly and meets the performance criteria for rapid water absorption, which meets the requirements for the use of curing materials within concrete.

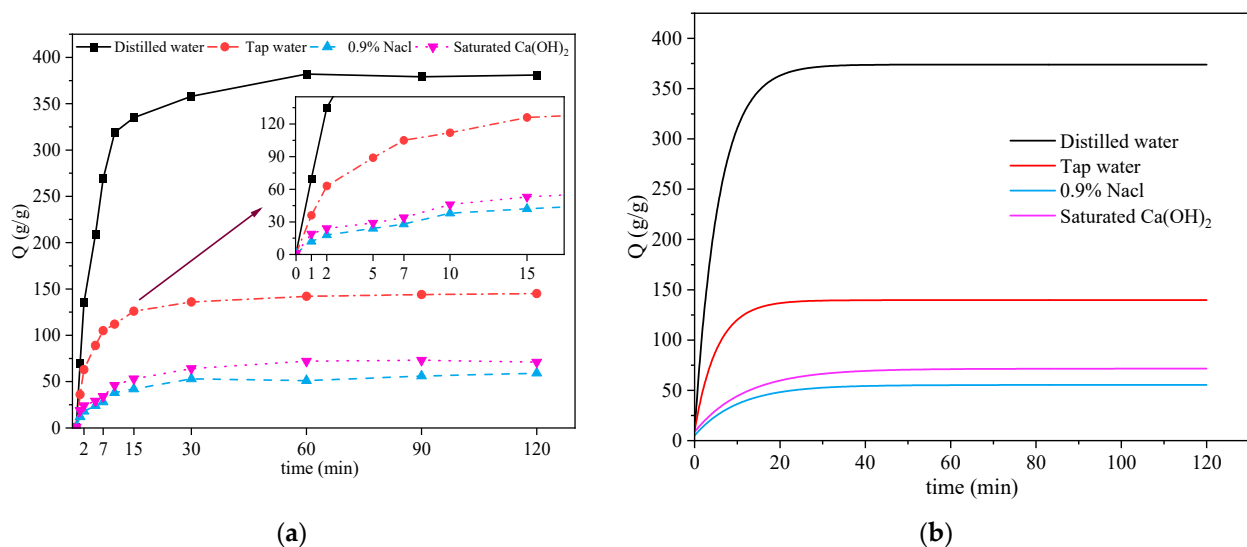


**Figure 9.** ATP-HEC-P (AA-co-AMPS): (a) the ATP-HEC-P (AA-co-AMPS) water retention at various temperatures, and (b) the fitting curves of water retention properties at different temperatures.

The swelling data of the prepared samples in various solutions are analyzed by nonlinear curve fitting and curves are plotted, as depicted in Figure 9b. The equations of the fitted curves and their corresponding  $R^2$  values are provided in Table 2. It is evident that the fitted curves closely approximate the actual data, with the minimum  $R^2$  value being 0.9740. These fitted equations can be utilized to estimate the water absorption capacity in different solutions over various periods and to assess the extent of water absorption.

**Table 2.** Expansion test fitting curve equations.

| Solution                          | Equation                                     | $R^2$  |
|-----------------------------------|--|--------|
| Deionized water                   | $Q = 373.96533 - 363.99687 \times 0.8393^t$  | 0.9923 |
| Tap water                         | $Q = 139.67793 - 129.44161 \times 0.83762^t$ | 0.9881 |
| 0.9% NaCl solution                | $Q = 55.31485 - 50.16333 \times 0.90708^t$   | 0.9740 |
| $\text{Ca}(\text{OH})_2$ solution | $Q = 71.49842 - 62.67467 \times 0.91952^t$   | 0.9895 |

### 3.7. Water Retention Properties

Upon reaching solvation equilibrium, ATP-HEC-P (AA-co-AMPS) comprises free water and bound water. Free water is easily volatilized. Bound water tightly holds to the material through hydrogen bonding and van der Waals force interactions, making it less susceptible to loss. Figure 10a illustrates ATP-HEC-P (AA-co-AMPS) water retention at varying temperatures. As observed in the figure, the water retention of ATP-HEC-P (AA-co-AMPS) exhibits a declining trend with increasing temperature and time. The water

retention rates are 85.90%, 78.65%, 72.18%, and 65.86% after 1 day, and 21.55%, 8.96%, 4.52%, and 2.52% after 7 days when ATP-HEC-P (AA-co-AMPS) is exposed to the environmental chamber at temperatures of 20 °C, 30 °C, 40 °C, and 50 °C. Additionally, in practice, other materials tend to cover the curing material inside the concrete, resulting in water retention properties that greatly exceed the experimental data obtained in a bare test environment, which ensures that ATP-HEC-P (AA-co-AMPS) meets the requirements for continuous water release inside the concrete.

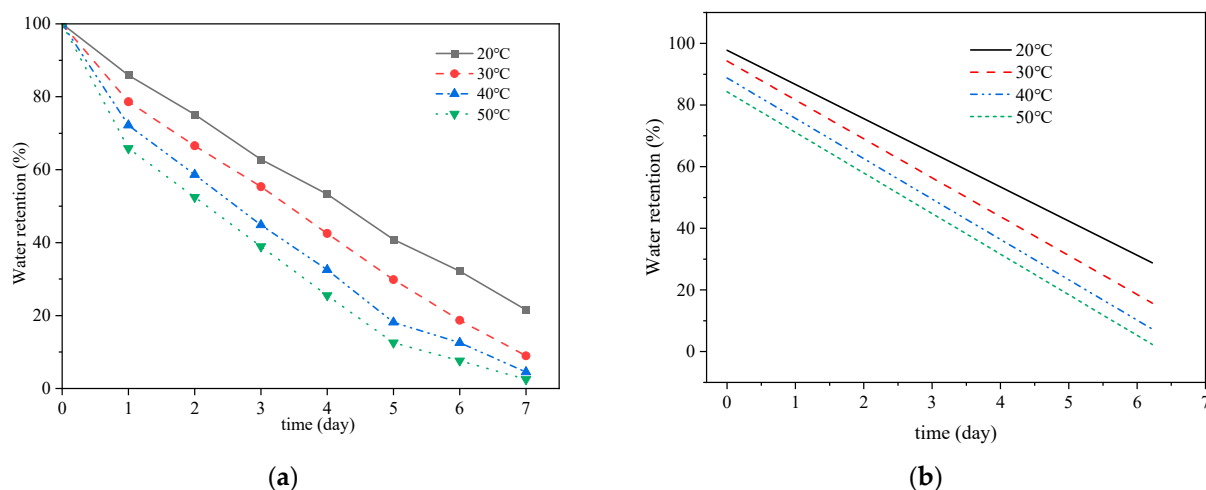


**Figure 10.** ATP-HEC-P (AA-co-AMPS) for (a) swelling test, (b) swelling test fitting curves.

Figure 10b illustrates the linearly fitted line segment for the water retention properties test, and the fitted equation and  $R^2$  values are provided in Table 3. The actual data closely resemble the fitted data, with the minimum  $R^2$  value being 0.9740. The water retention rate of the material at different temperatures over a period of 1 to 7 days can be estimated using the fitted equations.

**Table 3.** Water retention performance fitting equations.

| Temperature | Equation                   | $R^2$  |
|-------------|----------------------------|--------|
| 20 °C       | $R = 97.73417 - 11.07476t$ | 0.9969 |
| 30 °C       | $R = 84.2375 - 12.61714t$  | 0.9894 |
| 40 °C       | $R = 88.77833 - 13.09881t$ | 0.9568 |
| 50 °C       | $R = 84.31083 - 13.17631t$ | 0.9218 |

### 3.8. Repeated Swelling Properties

It is paramount for highly absorbent resins to exhibit repeatable swelling properties. This not only ensures sustainability but also reduces the overall cost associated with the material throughout its entire life cycle.

Figure 11 illustrates the repeated swelling tests conducted on the prepared samples. The figure demonstrates a significant degradation in the swelling properties of the material with an increasing number of repetitions, attributed to the destruction of the network structure resulting from successive expansions. Notably, the swelling data exhibit a clear stabilizing trend from the second to the third repetition. Subsequently, the removal of impurity ions from the structure due to concentration differences improves the liquid-absorbing capacity of ATP-HEC-P (AA-co-AMPS). The recurrent swelling performance of ATP-HEC-P (AA-co-AMPS) exhibits higher sensitivity to temperature changes, with the decrease in performance becoming increasingly apparent with rising temperatures. After five repetitions, the swelling at 20 °C, 30 °C, 40 °C, and 50 °C only reaches 78.75%, 70.90%, 66.82%, and 63.79% of the initial swelling. Since the hydration of cementitious materials in concrete is a long process, ATP-HEC-P (AA-co-AMPS) incorporated into concrete can

repeatedly absorb the water from the outside that seeps into the interior of the concrete structure many times, promoting the continuous hydration of cementitious materials.

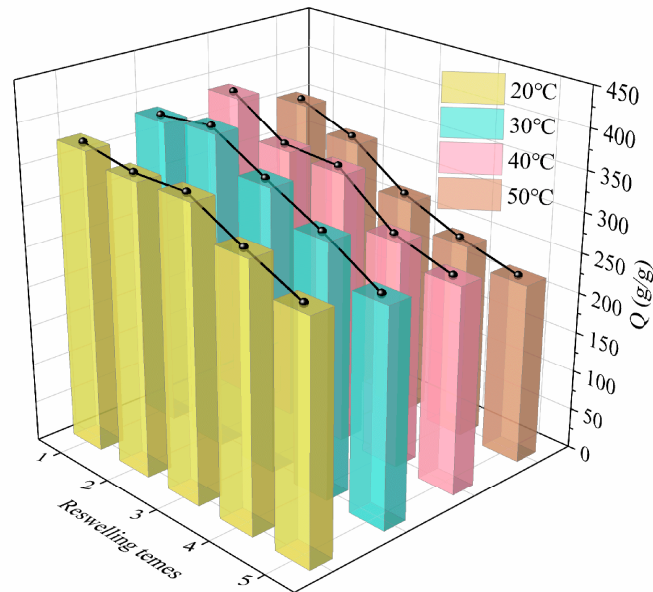


**Figure 11.** Repeated swelling tests on ATP-HEC-P (AA-co-AMPS) at different temperatures.

### 3.9. Swelling Capacity Test at Different pH Values

Concrete is currently alkaline, with the pH mostly between 7 and 12. In order to meet the requirements of a wider range of use, the liquid absorption capacity of ATP-HEC-P (AA-co-AMPS) was measured between pH 7 and 12, and the test results are shown in Figure 12. The liquid-absorbing ability of ATP-HEC-P (AA-co-AMPS) does not change much in the pH range of 7–10, and still shows good liquid-absorbing performance. When the pH value continues to increase, the liquid-absorbing capacity of ATP-HEC-P (AA-co-AMPS) begins to show a significant decreasing trend. However, the liquid-absorbing multiplicity is still 32 g/g at pH 12, which satisfies the requirement of in-concrete curing. The following two aspects may cause this situation. On the one hand, as the pH increases, -COOH in the polymer is transformed into -COO<sup>-</sup>, which may shield the negative charge of the -COO<sup>-</sup> anion due to the Na<sup>+</sup> ions in the solution, thus reducing the repulsive force of the polymer chain. On the other hand, the osmotic pressure disparity between the internal network and external solution decreases as the ionic strength of the swelling medium rises [37,38].

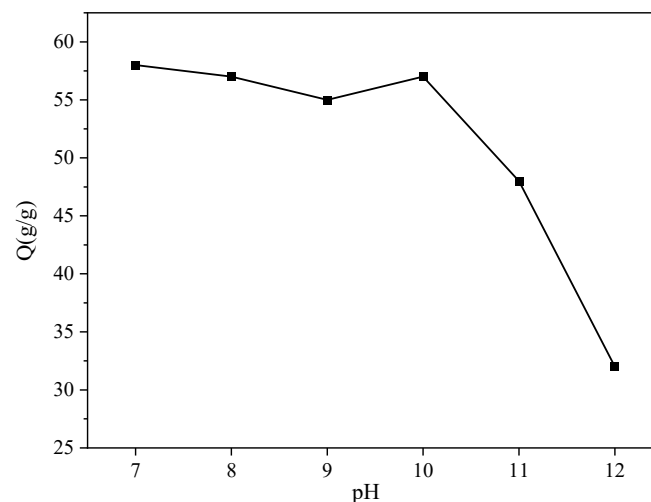


**Figure 12.** The dissolution multiplicity of samples as a function of the pH value.

### 3.10. Stress–Strain Curve Testing

Due to the complex structure inside the concrete and the harsh usage environment, the in-concrete curing agent is subjected to extrusion and friction in the usage process, thus putting higher requirements on the material's mechanical properties. To ensure the rigor of the experiments, the samples prepared in the molds were first cleaned with ethanol and deionized water, and then were directly subjected to stress–strain tests. As shown in Figure 13, the stress of the polymer modified by adding ATP increases from 4.25 N to 6.44 N with the same 50% deformation amount, and the mechanical strength increases by 35.7%. It can also be found that the HEC-P (AA-co-AMPS) changes significantly during the rebound process and shifts significantly from the compression curve. In contrast, the ATP-HEC-P (AA-co-AMPS) rebound curve almost coincides with the compression curve. These data indicate that the introduction of ATP improves the material's overall strength and makes it more robust for applications in complex environments.

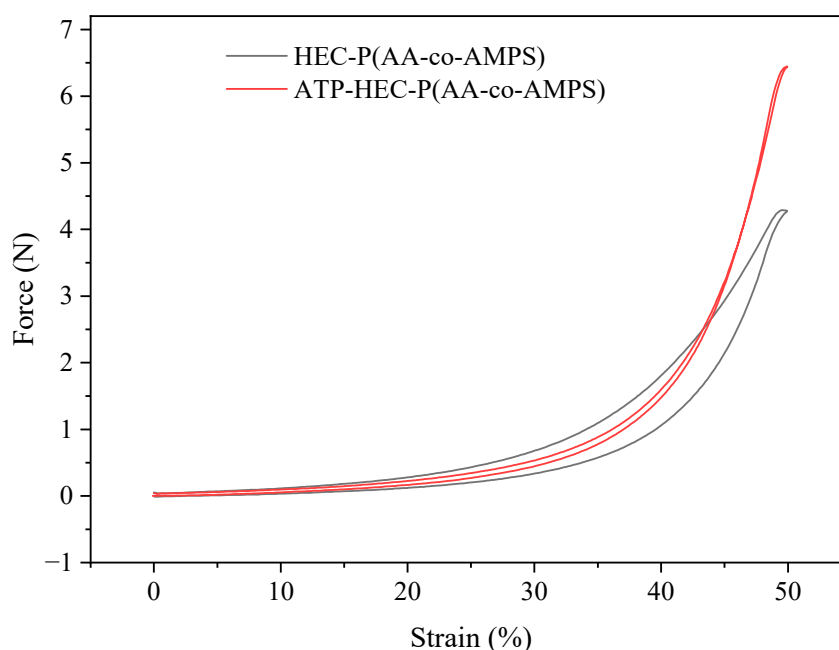


Figure 13. Stress–strain curves.

## 4. Conclusions

(1) SEM, FTIR, and thermal analyses demonstrated the successful polymerization of ATP-HEC-P (AA-co-AMPS), a concrete internal curing material synthesized using an aqueous solution. The water absorption multiplicity values in deionized water, tap water, 0.9% NaCl solution, and a saturated  $\text{Ca}(\text{OH})_2$  solution under the optimal preparation conditions were 382 g/g, 142 g/g, 57 g/g, and 73 g/g, which satisfy the requirements for the use of concrete internal curing agents.

(2) ATP-HEC-P (AA-co-AMPS) exhibited a rapid dissolution rate, reaching 80% of the dissolution multiplicity in approximately 15 min. It is possible to ensure that concrete slump and other properties are not affected by the increase in water consumption due to the addition of ATP-HEC-P (AA-co-AMPS).

(3) ATP-HEC-P (AA-co-AMPS) had excellent water retention performance, with a low water loss rate after 1 day, and could still adsorb a certain amount of water after 7 days in a 50 °C environment. This can ensure that ATP-HEC-P (AA-co-AMPS) will not release water completely in a short time after being mixed into the concrete, so as to achieve the purpose of long-term curing.

(4) ATP-HEC-P (AA-co-AMPS) exhibited a decrease in swelling multiplicity after five repeated swelling tests but maintained repeatable swelling, which helps to promote the hydration process of cementitious materials.

(5) ATP-HEC-P (AA-co-AMPS) showed no significant change in liquid absorption capacity in the pH value range of 7–10, and a significant decrease in the liquid absorption capacity occurred after the Ph value exceeded 10. However, it could still meet the requirements for in-concrete curing.

(6) After ATP modification, the mechanical strength of ATP-HEC-P (AA-co-AMPS) increased by 35.7% at 50% deformation, and the compression and rebound curves were almost coincident, which is more favorable for use in complex environments.

(7) Although the experimental data of ATP-HEC-P (AA-co-AMPS) are excellent, due to the time factor, there is no practical verification for the sample's effect on the concrete's performance after it is added to the concrete.

(8) Only the effect of ATP on the modification of HEC-P (AA-co-AMPS) was studied. There are still great prospects for studying clay minerals such as eclogite and bentonite on water-absorbing polymers.

**Author Contributions:** Conceptualization, Y.Z. and F.L.; methodology, Y.Z.; software, F.L.; validation, L.W., Y.L. and R.X.; formal analysis, F.L.; investigation, Y.Z.; resources, R.X.; data curation, Y.Z.; writing—original draft preparation, Y.Z.; writing—review and editing, R.X.; visualization, F.L.; supervision, Y.Z.; project administration, F.L.; funding acquisition, Y.Z. All authors have read and agreed to the published version of the manuscript.

**Funding:** This study was supported by the Science and Technology Department Project of Qinghai Province (Key R&D and Transformation Plan, Grant No. 2023-SF-124).

**Data Availability Statement:** The data used to support the findings of this study are included within the article.

**Conflicts of Interest:** Author Younan Zhao was employed by the company Qinghai Guoluo Highway Engineering Construction Co., Ltd. Authors Laifa Wang and Yongqing Li were employed by the company Qinghai Traffic Control Construction Engineering Group Co., Ltd. The remaining authors declare that the research was conducted in the absence of any commercial or financial relationships that could be construed as a potential conflict of interest.

## References

1. Khushbu; Warkar, S.G.; Kumar, A. Synthesis and assessment of carboxymethyl tamarind kernel gum based novel superabsorbent hydrogels for agricultural applications. *Polymer* **2019**, *182*, 121823. [[CrossRef](#)]
2. Guo, J.Z.; Shi, W.J.; Wang, P.H.; Hao, Q.G.; Li, J.K. Performance characterization of  $\gamma$ -poly (glutamic acid) super absorbent polymer and its effect on soil water availability. *Arch. Agron. Soil Sci.* **2022**, *68*, 1145–1158. [[CrossRef](#)]
3. Wang, Z.M.; Ning, A.M.; Xie, P.H.; Gao, G.Q.; Xie, L.X.; Li, X.; Song, A.D. Synthesis and swelling behaviors of carboxymethyl cellulose-based superabsorbent resin hybridized with graphene oxide. *Carbohydr. Polym.* **2017**, *157*, 48–56. [[CrossRef](#)]
4. Bardajee, G.R.; Hooshyar, Z.; Rastgo, F. Kappa carrageenan-g-poly (acrylic acid)/SPION nanocomposite as a novel stimuli-sensitive drug delivery system. *Colloid Polym. Sci.* **2013**, *291*, 2791–2803. [[CrossRef](#)]
5. Hou, S.J.; Sun, H.L.; Zhou, Y.H. Influence of super absorbent polymer on root characteristics and anchorage of *amorpha fruticosa* on rocky slope. *Appl. Sci.* **2022**, *12*, 2640. [[CrossRef](#)]
6. Malik, S.; Chaudhary, K.; Malik, A.; Punia, H.; Sewhag, M.; Berkesia, N.; Nagora, M.; Kalia, S.; Malik, K.; Kumar, D.; et al. Superabsorbent polymers as a soil amendment for increasing agriculture production with reducing water losses under water stress condition. *Polymers* **2023**, *15*, 161. [[CrossRef](#)]
7. Xiong, H.R.; Peng, H.; Ye, X.E.; Kong, Y.R.; Wang, N.; Yang, F.H.; Meni, B.; Lei, Z.Q. High salt tolerance hydrogel prepared of hydroxyethyl starch and its ability to increase soil water holding capacity and decrease water evaporation. *Soil Tillage Res.* **2022**, *222*, 105427. [[CrossRef](#)]
8. Zhang, W.X.; Liu, Q.; Liu, S.F.; Chen, J.; Guo, L.L.; Wang, P.; Lei, Z.Q. Study on seed emergence and seedling growth of *artemisia desertorum* with superabsorbent polymers. *Polymers* **2020**, *12*, 2873. [[CrossRef](#)]
9. Yang, J.; Wang, J.F.; Su, Y.; He, X.Y.; Wang, F.L.; Liang, W. On the factors affecting the swelling behavior of superabsorbent polymers in cement-related environment. *Constr. Build. Mater.* **2023**, *409*, 133938. [[CrossRef](#)]
10. Ismaeilimoghadam, S.; Jonoobi, M.; Ashori, A.; Shahraki, A.; Azimi, B.; Danti, S. Interpenetrating and semi-interpenetrating network superabsorbent hydrogels based on sodium alginate and cellulose nanocrystals: A biodegradable and high-performance solution for adult incontinence pads. *Int. J. Biol. Macromol.* **2023**, *253*, 127118. [[CrossRef](#)]
11. Mistry, P.A.; Konar, M.N.; Latha, S.; Chadha, U.; Bhardwaj, P.; Eticha, T.K. Chitosan superabsorbent biopolymers in sanitary and hygiene applications. *Int. J. Polym. Sci.* **2023**, *2023*, 4717905. [[CrossRef](#)]

12. Pourjavadi, A.; Fakoorpoor, S.M.; Hosseini, P.; Khaloo, A. Interactions between superabsorbent polymers and cement-based composites incorporating colloidal silica nanoparticles. *Cem. Concr. Compos.* **2013**, *37*, 196–204. [[CrossRef](#)]
13. Ai, F.J.; Yin, X.Z.; Hu, R.C.; Ma, H.L.; Liu, W. Research into the super-absorbent polymers on agricultural water. *Agric. Water Manag.* **2021**, *245*, 106513. [[CrossRef](#)]
14. Olad, A.; Gharekhani, H.; Mirmohseni, A.; Bybordi, A. Synthesis, characterization, and fertilizer release study of the salt and pH-sensitive NaAlg-g-poly(AA-co-AAm)/RHA superabsorbent nanocomposite. *Polym. Bull.* **2017**, *74*, 3353–3377. [[CrossRef](#)]
15. Sousa, H.R.; Lima, I.S.; Neris, L.M.L.; Silva, A.S.; Nascimento, A.; Araújo, F.P.; Ratke, R.F.; Silva, D.A.; Osajima, J.A.; Bezerra, L.R.; et al. Superabsorbent hydrogels based to polyacrylamide/cashew tree gum for the controlled release of water and plant nutrients. *Molecules* **2021**, *26*, 2680. [[CrossRef](#)] [[PubMed](#)]
16. Wali, S.; Khattak, M.I.; Khattak, M.I.; Sjjad, A. Synthesis, characterization and application of Karak bentonite clay-graft-poly (Acrylamide/Co- Acrylic Acid) superabsorbent Composite and its adsorption study for selected heavy metals. *J. Chem. Soc. Pak.* **2023**, *45*, 226–236.
17. Hao, Y.; Qu, J.; Tan, L.; Liu, Z.Y.; Wang, Y.C.; Lin, T.R.; Yang, H.; Peng, J.; Zhai, M.L. Synthesis and property of superabsorbent polymer based on cellulose grafted 2-acrylamido-2-methyl-1-propanesulfonic acid. *Int. J. Biol. Macromol.* **2023**, *233*, 123643. [[CrossRef](#)] [[PubMed](#)]
18. Zhang, H.; Zhang, X.; Qiao, S.P.; Wang, B.; Zeng, X.; Ren, B.; Yang, X.D. Modified corn stalk carboxymethyl cellulose, acrylic acid and SBA-15 based composite hydrogel used for agricultural water retention. *J. Appl. Polym. Sci.* **2023**, *140*, e54613. [[CrossRef](#)]
19. Moohan, J.; Stewart, S.A.; Espinosa, E.; Rosal, A.; Rodríguez, A.; Larrañeta, E.; Donnelly, R.F.; Domínguez-Robles, J. Cellulose nanofibers and other biopolymers for biomedical applications. A review. *Appl. Sci.* **2020**, *10*, 65. [[CrossRef](#)]
20. Tan, Q.; Chen, H.; Chang, H.Q.; Woo, M.W.; Liu, W.T. Current advances in design of starch-based superabsorbent polymers and their removal of typical pollutants from tannery wastewater. *Starch-Starke* **2023**, *75*, 2300004. [[CrossRef](#)]
21. Wang, Y.Q.; Fu, E.F.; Saghri, S.; Xiao, Z.G. Novel superabsorbent polymer composite embedded with sodium alginate and diatomite for excellent water absorbency, water retention capacity, and high thermal stability. *J. Mol. Struct.* **2024**, *1300*, 137244. [[CrossRef](#)]
22. Huang, X.M.; Ao, X.; Yang, L.H.; Wang, C.W.; Meng, L.L. One-pot freezing-thawing preparation of hydroxyethyl cellulose reinforced polyvinyl alcohol based ionic hydrogel. *Integr. Ferroelectr.* **2023**, *231*, 106–114. [[CrossRef](#)]
23. Liu, X.Y.; Gan, J.Y.; Huang, Y.; Liu, J.P.; Pu, D.D.; Li, X.; Wang, M.S.; Lin, Y.H. Gel polymer electrolyte based on polymer matrix of hydroxyethyl cellulose composite lignocellulose. *Bull. Mater. Sci.* **2023**, *46*, 211. [[CrossRef](#)]
24. Kwon, Y.R.; Kim, H.C.; Kim, J.S.; So, J.H.; Chang, Y.W.; Kim, D.H. Semi-IPN superabsorbent polymer based on itaconic acid and polyvinyl alcohol with improved gel strength and salt resistance. *Polym. Eng. Sci.* **2023**, *63*, 1943–1952. [[CrossRef](#)]
25. Wei, B.G.; Cheng, X.B.; Wang, G.; Li, H.; Song, X.S.; Dai, L. Graphene oxide adsorption enhanced by attapulgite to remove Pb (II) from aqueous solution. *Appl. Sci.* **2019**, *9*, 1390. [[CrossRef](#)]
26. Liu, S.; Fan, F.Q.; Liu, X.F.; Guo, Y.; Ni, Z.K.; Wang, S.R. Old wine and new bottles: Insights into traditional attapulgite adsorbents with functionalized modification strategies applied in efficient phosphate immobilization. *J. Clean. Prod.* **2023**, *395*, 136451. [[CrossRef](#)]
27. Cui, X.C.; Zhong, Z.Y.; Xie, X.D.; Jiang, P.H. Sorptive removal of cadmium using the attapulgite modified by the combination of calcination and iron. *Environ. Sci. Pollut. Res.* **2023**, *30*, 120820–120831. [[CrossRef](#)]
28. Busuioc, C.; Isopencu, G.O.; Deleanu, I.M. Bacterial cellulose-polyvinyl alcohol based complex composites for controlled drug release. *Appl. Sci.* **2023**, *13*, 1015. [[CrossRef](#)]
29. Phonlakan, K.; Meetam, P.; Chonlaphak, R.; Kongseng, P.; Chantarak, S.; Budsombat, S. Poly(acrylic acid-co-2-acrylamido-2-methyl-1-propanesulfonic acid)-grafted chitosan hydrogels for effective adsorption and photocatalytic degradation of dyes. *RSC Adv.* **2023**, *13*, 31002–31016. [[CrossRef](#)]
30. You, X.Y.; Xiao, X.; Zhao, Y.; Zhu, X.L.; Li, X.P.; Zhang, H.J. Highly swellable hydrogel from neutral hydroxyethyl cellulose for human weight control. *ACS Appl. Polym. Mater.* **2023**, *5*, 9425–9432. [[CrossRef](#)]
31. Tamer, Y.B. A new design of poly (N-isopropylacrylamide) hydrogels using biodegradable poly (beta-aminoester) crosslinkers as fertilizer reservoirs for agricultural applications. *Gels* **2023**, *9*, 127. [[CrossRef](#)]
32. Ghasri, M.; Jahandideh, A.; Kabiri, K.; Bouhendi, H.; Zohuriaan-Mehr, M.J.; Moini, N. Glycerol-lactic acid star-shaped oligomers as efficient biobased surface modifiers for improving superabsorbent polymer hydrogels. *Polym. Adv. Technol.* **2019**, *30*, 390–399. [[CrossRef](#)]
33. He, G.H.; Ke, W.W.; Chen, X.; Kong, Y.H.; Zheng, H.; Yin, Y.H.; Cai, W.Q. Preparation and properties of quaternary ammonium chitosan-g-poly(acrylic acid-co-acrylamide) superabsorbent hydrogels. *React. Funct. Polym.* **2017**, *111*, 14–21. [[CrossRef](#)]
34. Li, Q.L.; Lu, H.X.; Xiao, H.Y.; Gao, K.S.; Diao, M.M. Adsorption capacity of superabsorbent resin composite enhanced by non-thermal plasma and its adsorption kinetics and isotherms to lead ion in water. *J. Environ. Chem. Eng.* **2013**, *1*, 996–1003. [[CrossRef](#)]
35. Xu, Z.; Fei, Q.; Zhang, X. Synthesis of the starch grafting of superabsorbent and high oil-absorbing resin. *J. Environ. Sci.* **2013**, *25*, S97–S100. [[CrossRef](#)]
36. Zhu, W.J.; Zhang, Y.G.; Wang, P.L.; Yang, Z.Y.; Yasin, A.; Zhang, L.T. Preparation and applications of salt-resistant superabsorbent poly (acrylic acid-acrylamide/fly ash) composite. *Materials* **2019**, *12*, 596. [[CrossRef](#)]

37. Wang, J.L.; Wang, W.B.; Wang, A.Q. Synthesis, characterization and swelling behaviors of hydroxyethyl cellulose-g-poly (acrylic acid)/Attapulgite superabsorbent composite. *Polym. Eng. Sci.* **2010**, *50*, 1019–1027. [[CrossRef](#)]
38. Deng, C.H.; Zhai, X.M.; Li, W.R.; Xiong, R.; Lu, F.Y. Preparation and properties of attapulgite/brucite fiber-based highly absorbent polymer composite. *Materials* **2024**, *17*, 1913. [[CrossRef](#)]

**Disclaimer/Publisher’s Note:** The statements, opinions and data contained in all publications are solely those of the individual author(s) and contributor(s) and not of MDPI and/or the editor(s). MDPI and/or the editor(s) disclaim responsibility for any injury to people or property resulting from any ideas, methods, instructions or products referred to in the content.